# Sequence- and Stereospecific Conformational Rearrangement of Styrene Oxide Adducts Located at A·C Mismatched Base Pairs†

Mario F. Simeonov,*,‡ Pamela J. Tamura,§ Amanda S. Wilkinson,§ Constance M. Harris,§ Thomas M. Harris,§ and Michael P. Stone*,§

*Institute of Organic Chemistry with Center of Phytochemistry, Bulgarian Academy of Sciences, BG 1113 Sofia, Bulgaria, and Department of Chemistry and Center in Molecular Toxicology, Vanderbilt University, Nashville, Tennessee 37235*

*Received September 3, 1999; Revised Manuscript Received November 12, 1999*

ABSTRACT: The solution structures of R- and S-α-($N^6$-adenyl)-styrene oxide adducts mismatched with cytosine at position $X^7$ in d(CGGACAXGAAG)·d(CTTCCTGTCCG), incorporating codons 60, 61 (underlined), and 62 of the human *N-ras* protooncogene, were determined. These were the R- and S(61,3)C adducts. The structures for these mismatched adducts differed from the sequence isomeric R- and S(61,2)C adducts [Painter, S. L., Zegar, I. S., Tamura, P. J., Bluhm, S., Harris, C. M., Harris, T. M., and Stone, M. P. (1999) *Biochemistry 38*, 8635−8646]. The results reveal that the structural consequences of cytosine mispairing opposite the R- and S-α-SO adducts differ as a function of DNA sequence. The thermodynamic stability of both the R- and S(61,3)C mismatched adducts was dependent upon pH. At neutral pH, the R- and S(61,3)C adducts exhibited significant structural perturbation and had lower $T_m$ values, as compared to the R- and S(61,2)C adducts. In both instances, this was attributed to reorientation about the C6−$N^6$ bond, such that the $N^6$H proton faced away from the Watson−Crick face of the purine base and into the major groove. The conformation about the $N^6-C_\alpha-C_\beta-O$ torsion angle was predicted from rMD calculations to be stabilized by a N/O gauche-type interaction between the styrenyl hydroxyl moiety and adenine $N^6$ at the lesion site. For the R(61,3)C adduct, the styrenyl moiety remained oriented in the major groove and faced in the 3′-direction. In the properly base-paired R(61,3) adduct, it had faced in the 5′ direction. For the S(61,3)C adduct, the styrene ring was inserted into the duplex, approximately perpendicular to the helical axis of the DNA. It faced in the 5′-direction. In the properly base-paired S(61,3) adduct, it had faced in the 3′-direction. The results were correlated with site-specific mutagenesis experiments in vivo. The latter revealed that the R- and S(61,3)-α-styrene oxide adducts were nonmutagenic. This may be a consequence of the greater structural perturbation associated with formation of the cytosine mismatch at neutral pH for the R- and S(61,3) adducts as compared to the S(61,2) adduct that exhibited low levels of A → G mutations.

Styrene, a mutagen in prokaryotes (*1*, *2*) and eukaryotes (*3*), is of concern as a potential human mutagen (*4*−*7*). Styrene genotoxicity results from cytochrome $P_{450}$-mediated metabolism to the ultimate carcinogenic species, styrene oxide (SO)[1] (*8*−*15*). Styrene oxide reacts in vitro to form adducts at a number of nucleophilic sites in DNA, including the R- and S-α-adducts at the exocyclic amino groups of guanine (*16*) and adenine (*17*). The adenyl $N^6$ adducts arise in vitro both from direct reaction at the exocyclic carbon and as a consequence of Dimroth rearrangement following reaction at N1 (*18*) (Scheme 1). The reaction of styrene oxides with the exocyclic amino groups of guanosine (*19*) and adenine (*18*) exhibited considerable $S_N1$ character, but favored inversion of stereochemistry.

SO induces sister chromosome exchange and aberrations in human lymphocytes in vitro (*20*, *21*). Adducts of SO at guanine $O^6$ and guanine $N^2$ were identified in human cells (*22*−*25*). Increased levels of the guanine $O^6$ adduct, a potential biomarker for styrene exposure, were observed in lamination workers chronically exposed to styrene in the

† This research was supported by NIH Grant ES-05509 (M.P.S.). Funding for the NMR spectrometer was supplied by a grant from the NIH shared instrumentation program, RR-05805, and the Vanderbilt Center in Molecular Toxicology, ES-00267. This study made use of the National Magnetic Resonance Facility at Madison. NMRFAM equipment was purchased with funds from the University of Wisconsin, NSF Grants DMB-8415048 and BIR-9214394, NIH Grants RR-02301, RR-02781, RR08438, and the USDA.

* To whom correspondence should be addressed. (M.F.S.) Phone: +359 2 724 817. Fax: +359 2 700 225. E-mail: mario@orgchm.bas.bg. (M.P.S.) Phone: (615) 322-2589. Fax: (615) 343-1234. E-mail: stone@toxicology.mc.vanderbilt.edu.

‡ Institute of Organic Chemistry with Center of Phytochemistry.

§ Department of Chemistry and Center in Molecular Toxicology.

[1] Abbreviations: DSS, 2,2-dimethyl-2-silapentane-5-sulfonate; EDTA, ethylenediaminetetraacetic acid; HPLC, high-pressure liquid chromatography; MD, molecular dynamics; rMD, restrained molecular dynamics; NMR, nuclear magnetic resonance; NOE, nuclear Overhauser enhancement; NOESY, two-dimensional NOE spectroscopy; PAH, polycyclic aromatic hydrocarbon; ppm, parts per million; SO, styrene oxide; TPPI, time proportional phase increment; TOCSY, total homonuclear correlated spectroscopy; 1D, one-dimensional; 2D, two-dimensional. A, C, G, and T refer to mononucleotide units; $^{R-SO}$A is the R-α-styrene oxide modified nucleotide; $^{S-SO}$A is the S-α-styrene oxide modified nucleotide. A right superscript refers to numerical position in the oligodeoxynucleotide sequence starting from the 5′-terminus of chain A and proceeding to the 3′-terminus of chain A and then from the 5′-terminus of chain B to the 3′-terminus of chain B.

10.1021/bi992080t CCC: $19.00 
Published on Web 01/14/2000

Scheme 1: Structures of the R- and S-α-(N$^6$-adenyl) Styrene Oxide Adducts

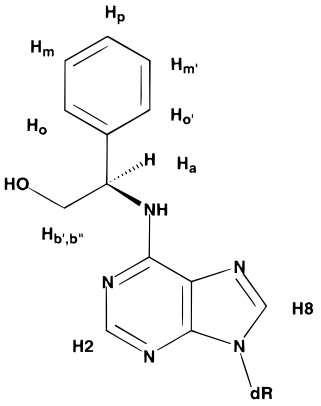


**R-α-(N$^6$-adenyl)-styrene oxide adduct**

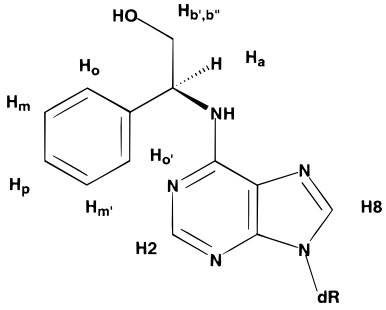


**S-α-(N$^6$-adenyl)-styrene oxide adduct**

plastics industry (*26*). Molecular analysis of mutations at the hypoxanthine-guanine phosphoribosyl transferase (*hprt*) gene in peripheral blood lymphocytes suggested that they occurred at both guanine and adenine sites, and were predominantly base pair substitutions (*27*). The occurrence of guanine O$^6$ adducts did not strongly correlate with the frequency of *hprt* mutations (*26*). This suggested that the guanine O$^6$ SO adducts were weakly mutagenic. Alternatively, they were perhaps not the source of the mutations. Thus, the relationship between styrene-induced DNA damage and mutagenesis remains to be established (*25*).

Cells containing activated oncogenes often, but not always, contain mutations in *ras* (*28*). Therefore, it was decided to examine the R- and S-α-SO adducts (Scheme 1) located at the exocyclic amino groups of adenines in the *ras61* oligodeoxynucleotide d(CGGACAAGAAG)·d(CTTCTTGTCCG). This oligodeoxynucleotide was derived from the codon 61 sequence (underlined) of the human *N-ras* protooncogene (Scheme 2). Potential SO-induced mutations in *ras* are expected to contribute to cellular transformation. Because carcinogenesis is a multistep process (*29*, *30*), the precise biological consequences of SO-induced mutations at specific sites in individual cells are difficult to determine. These are expected to differ from one cell to the next, depending upon the overall genetic background of the specific somatic cells in which mutations occur. Both the nature and sequential order of genetic changes modulate tumor morphology and the likelihood of tumor progression (*31*); consequently, mutations induced by SO will not necessarily be rate limiting in carcinogenesis.

Site-specific mutagenesis studies in which the *ras61* sequence was modified at the S(61,2) position revealed that

Scheme 2: R(61,3)C and S(61,3)C Mismatched Oligodeoxynucleotides, Where R = R-α-(*N*$^6$-adenyl)-styrene Oxide and S = S-α-(*N*$^6$-adenyl)-styrene Oxide Adduct, Respectively.

ras codons

```
                60          61          62
5'-C1 |G2 G3 A4 |C5 A6 R7 |G8 A9 A10|G11-3'
3'-G22|C21C20T19|G18T17C16|C15T14T13|C12-5'

                60          61          62
5'-C1 |G2 G3 A4 |C5 A6 S7 |G8 A9 A10|G11-3'
3'-G22|C21C20T19|G18T17C16|C15T14T13|C12-5'
```

the adenyl N$^6$ lesion was weakly mutagenic. Low levels of A → G transitions were observed (*32*). This was the most frequently observed SO-induced *hprt* mutation in human lymphocytes (*27*), which suggested the potential importance of the adenyl N$^6$ lesions in understanding the toxicology of SO. Thus, while the guanine O$^6$ adducts potentially provide a biomarker of exposure, the less common adenine N$^6$ lesions might be more mutagenic (*27*). The bulkier and intercalating adenyl N$^6$ adducts of benzo[*a*]pyrene (*33*) and benz[*a*]anthracene (*34*) also yielded A → G mutations, but at greater levels. To develop a better understanding of the relationship between adduct structure and activity at adenine N$^6$, it was of interest to examine whether a structural basis could be discerned for the induction of A → G mutations by SO. A potential explanation for these mutations was that SO adduction facilitated formation of wobble pairing between protonated adenine and cytosine (*35*−*46*). Alternatively, SO adduction might perturb the geometry of the adducted adenine so that the replication complex misinserted cytosine during replication.

The unmodified *ras61* oligodeoxynucleotide (*47*) existed as a right-handed B-DNA-like duplex. The structures of the R- and S(61,2)- and the R- and S(61,3)-α-styrene oxide lesions in the *ras61* oligodeoxynucleotide (*48*−*50*) revealed the influence of stereochemistry in determining adduct orientation. The R-diastereomer was consistently oriented in the 5′-direction while the S-diastereomer was oriented in the 3′-direction from the lesion site. Studies of R- and S-α-(N$^6$-adenyl)-styrene oxide adducts at position X$^6$, mismatched with cytosine, showed that surprisingly, and unlike the unmodified *ras61* (61,2) A·C mismatch, neither the R- nor the S(61,2)C SO adducts formed protonated A·C pairs (*51*). Furthermore, $^1$H NMR spectroscopy and UV melting data revealed that unlike the R(61,2) adduct which existed as a single conformation in which the styrenyl moiety was oriented in the 5′-direction in the major groove from the lesion site (*48*, *50*), the R(61,2)C adduct was disordered. In contrast, the S(61,2)C adduct existed as a single species in solution and yielded a refined solution structure, whereas the S(61,2) adduct had equilibrated between multiple conformations (*49*, *50*). NOESY data revealed that the phenyl ring of the styrene moiety was located in the major groove of the DNA and oriented in the 3′-direction. A shift of the modified adenine toward the minor groove resulted in the styrenyl ring stacking with nucleotide C$^5$ on the 5′-side of the lesion, which had shifted toward the major groove. This adduct-induced change in base-pairing geometry provided a possible explanation for the low levels of A → G mutations

observed for the S(61,2) adduct, which were not observed for the R(61,2) adduct (*32*).

The results of the present work reveal a striking sequence-dependence effect in the conformations of the corresponding modified X·C mismatches when located at the R- or S(61,3)C positions in the *ras61* oligodeoxynucleotide. In contrast to the R- and S(61,2)C mismatches (*51*), the R- and S(61,3)C mismatches exhibited the pH dependence characteristic of the unadducted (61,2)C mismatch. Moreover, the NMR data suggested that at neutral pH and when placed opposite to a mismatched cytosine in the complementary strand, the energetically favored adducted structures underwent rotation about the C6−$N^6$ bond. Consequently, the aromatic styrenyl moieties were oriented in the opposite directions as compared to the heretofore observed major groove styrenyl adducts. In the mismatched adduct, the R−SO moiety remained in the major groove but was oriented in the 3′-direction from the site of adduction. The S−SO moiety was oriented in the 5′-direction from the site of adduction, accompanied by insertion of the styrenyl ring into the DNA duplex approximately perpendicular to the helical axis of the DNA duplex. This resulted in distortion of the DNA at the site of adduction. The results reveal the exquisite thermodynamic balance between Watson−Crick hydrogen bonding vs non-Watson−Crick hydrogen bonding and DNA sequence.

## MATERIALS AND METHODS

*Oligodeoxynucleotides*. The unmodified oligodeoxynucleotide 5′-d(CGGACAAGAAG)-3′ and its mismatch complement 5′-d(CTTCCTGTCCG)-3′ were purchased from the Midland Certified Reagent Company (Midland, TX). The SO-adducted oligodeoxynucleotides were prepared and purified as reported (*52*). Enzyme digest and circular dichroism (CD) analyses were performed to verify the stereochemistry of the adducted oligodeoxynucleotides. The concentrations of the single-stranded oligodeoxynucleotides were determined from the extinction coefficients (*53*), $9.71 \times 10^{-4}$ and $8.73 \times 10^4$ $M^{-1}$ $cm^{-1}$, respectively. Equimolar amounts were mixed and annealed in 10 mM $NaH_2PO_4$, 0.1 M NaCl, and 50 $\mu$M $Na_2EDTA$ at pH 6.9. The annealed duplex was eluted from a hydroxylapatite column using sodium phosphate. The samples were desalted using gel filtration (Bio-Gel G-25, Bio-Rad, Inc., Hercules, CA).

*UV Melting.* The experiments were carried out on a Varian Cary 4E spectrophotometer. The samples were dissolved in 10 mM $NaH_2PO_4$, 0.05 mM $Na_2EDTA$, and 1 M NaCl buffer at pH 5.7, pH 7.0, and pH 8.5. The concentrations were adjusted to $4.8 \times 10^{-6}$ M in 1 cm cuvettes. The temperature was increased at a rate of 0.5 °C/min from 2 to 85 °C. Absorbance was measured at 260 nm. The melting temperatures of the native and modified oligodeoxynucleotides were calculated by determining the midpoints of the melting curves from the first-order derivatives.

*NMR Spectroscopy*. Spectra were recorded at $^1$H frequencies of 750.13 and 500.13 MHz. Nonexchangeable resonance assignments were made from phase-sensitive NOESY (TPPI quadrature detection) at $t_m = 80$, 180, 250, and 350 ms, and phase-sensitive DQF-COSY and TOCSY ($t_m = 40$ and 80 ms) spectra in $D_2O$, at temperatures between 288 and 298 K. Spectra were processed using FELIX (version 97.0, Molecular Simulations, Inc., San Diego, CA) on Octane workstations (Silicon Graphics, Inc., Mountain View, CA). The relaxation delay was 2 s. The data (2K × 512) were zero-filled to give matrix of 2K × 1K (4K × 2K for DQF-COSY) real points. A skewed sinebell-square apodization function with a 90° phase-shift was used in both dimensions. 2D NOESY with WATERGATE (*54*) solvent suppression and TPPI in the $t_1$ dimension was used in 90% $H_2O$ solvent for detection of exchangeable proton resonances.

*Experimental Restraints. (a) Distance Restraints.* Footprints were selected manually to fit NOE cross-peaks at the contour level chosen which showed the weak NOEs but not the random noise. For overlapped cross-peaks, footprints were estimated and larger upper and lower error bounds were assigned to the resulting distances. Canonical A- and B-DNA structures were generated using INSIGHTII (Molecular Simulations, Inc., San Diego, CA) and served as reference structures for establishing an initial intensity matrix. The styrene moiety was incorporated into initial structures by bonding the styrene oxide benzylic carbon to $N^6$ of adenine, with appropriate stereochemistry. These structures were energy minimized, using X-PLOR (*55*), for 100 iterations by the conjugate gradient method to give the starting structures IniA and IniB. For each of the three mixing times, the experimental NOE-derived distances were combined with the initial intensity matrix to generate a hybrid intensity matrix using MARDIGRAS (*56*, *57*). The hybrid intensity matrix was constructed assuming isotropic molecular motion, with correlation values, $\tau_c$, of 2 and 3 ns for both sugar and base protons, at each NOE mixing time. The resulting distance sets were pooled; average values of all minimum and maximum distances were used in setting error bounds to give the experimental NOE restraints used in subsequent molecular dynamics calculations (*58*).

*(b) Torsion Angle Restraints.* Dihedral angle constraints in the deoxyribose sugar rings were obtained from $^aJ(1',2'')$, $^pJ(1',2')$, and $^aJ(2',3')$ coupling constants and the sums of coupling constants, Σ1′, Σ2′, Σ2″, Σ3′, and Σ4′ from DQF-COSY cross-peak patterns (*59*, *60*). The coupling constants established ranges of the pseudorotation angle (*61*), and these in turn were converted into specific constraints on the angles $\nu_0$, $\nu_1$, $\nu_2$, $\nu_3$, and $\nu_4$ (*62*). The minimum range of these constraints was held to ±5°. Torsion angle $\delta$ was determined from experimental NOE distance and sugar ring torsion restraints. The following examination for $\gamma$ was performed (*61*). The $\Sigma J_{H4'}$ from DQF-COSY spectra (where it could be measured) was <10 Hz. The sum of H4′ J coupling ($\Sigma J_{H4'} = J_{H4'-H3'} + J_{H4'-H5'} + J_{H4'-H5''}$) depended on the sugar pseudorotation P and $\gamma$. The sum $J_{H4'-H5'} + J_{H4'-H5''}$ was >12.5 Hz in the case of $\gamma^t$ or $\gamma^{g-}$ and <4 Hz in the case where $\gamma$ was ∼60° ($\gamma^{g+}$). In the latter case ($\gamma^{g+}$ conformation), the cross-peak H6(H8) → H5′,H5″ cross-peak is not observable, as we found. The H4′ NOESY ($t_m$=80 ms) line width provided information on $\Sigma J_{H4'}$. For most sugars, the H4′ $\nu_{1/2}$ determined from F2 slices of the NOESY spectrum was in the range 9.5−14.5 Hz. This analysis restricted $\gamma$ to the 10−110° range and justified the loose restraints of 60 ± 50° that were employed. The angle $\epsilon$ was related to the $^{31}$P−$^1$H 3 bond J coupling ($J_{HCOP}$). Moreover, $\Sigma J_{H3'} = (J_{H3'-H4'} + J_{H3'-H2'} + J_{H3'-H2''} + J_{HCOP})$ from DQF-COSY spectra (where it could be measured) (*61*) was found to lie in the 10−14 Hz range. The minimal sum of $^1$H−$^1$H *J* coupling constants in the case (S-type sugar

pseudorotation) is ~7 Hz, and hence the maximum possible $J_{HCOP}$ were all measured in the 3−7 Hz range. Then, the allowable ranges for $\epsilon$ were either 130−240° (a $B_I$ type phosphate) or 270−300° (a $B_{II}$ type phosphate). These indirectly derived $J_{HCOP}$ were compared with those measured via H3′ selective $^1H$-$^{31}P$ correlation experiments. The latter were in the 8−13 Hz range, which agreed with the observation that when the line width was greater than the scalar interactions, partial cancellation occurred since positive and negative peaks were superimposed (*63*). The angle $\chi$ was determined from intranucleotide distances between the base H6 (or H8 and H5) to sugar H1′ (or H2′, H2″, and H3′) protons. Only the base−H1′ distance was directly dependent on $\chi$; the other distances were dependent on the combination of $\chi$ and sugar pseudorotation. Two independent base-to-sugar proton distances plus the sugar pseudorotation determined $\chi$. Because the sugar ring pseudorotation was defined, the analysis was performed by a NOESY experiment at $t_m$ = 80 ms, checking qualitatively the intensity of H6(H8)/H1′ and H6(H8)/H2′ cross-peaks. The intensity of the former cross-peaks decreased, while those of the latter (often overlapped) remained stronger. Theoretically, the first distances were ~4 Å (for $\chi_{anti}$) and ~2.5 Å (for $\chi_{syn}$), while the latter were ~2 Å (for $\chi_{anti}$) and ~4.5 Å (for $\chi_{syn}$). Thus, the backbone torsion angles α, $\beta$, $\gamma$, $\epsilon$, and $\zeta$ were restricted to broad ranges of $-70 \pm 50°$, $180 \pm 50°$, $-60 \pm 50°$, $180 \pm 50°$, and $-70 \pm 50°$, respectively.

*Structure Refinement*. INSIGHT II was used to build starting A- and B-DNA structures and for molecular visualization. Potential energy minimization and rMD calculations were performed using X-PLOR (version 2.4) (*55*), based on the CHARMM (*64*) force field. The effective energy term comprised restraining terms that used experimental distance information. The empirical energy consisted of terms for bonds, bond angles, dihedral angles, chirality or planarity, hydrogen bonding, and nonbonded (van der Waals and electrostatic) terms. The distance restraints were divided into five classes based on the confidence factor obtained from MARDIGRAS.

After initial energy minimization starting with IniA or IniB DNA structures and 5 ps high temperature (900 K) with force constants set at 20 kcal/mol $A^2$ (for dihedral restraints), 10 kcal/mol $A^2$ (for base pair restraints), and 50, 45, 40, 35, and 30 kcal/mol $A^2$ (for the five classes distance restraints), 3 ps of high-temperature dynamics with scaling force constants set up to 100 (for dihedral and base pair restraints) and up to 150 kcal/mol $A^2$ (for the distance restraints) was run. These conditions were kept for another 3 ps. This was followed by 3 ps cooling dynamics to 300 K with high force constants, 3 ps cold-high dynamics, 3 ps scaling down force constants to their original values, and 10 ps final-cold dynamics. The integration time step was 1 fs; structure coordinates were achieved every 0.1 ps. The emergent structures were averaged and potential energy minimized to obtain the final structure. Back-calculation of theoretical cross-peak intensities from the emergent structures was performed using CORMA (version 4.0) (*65*). The agreement between the experimental cross-peak intensities and the values calculated from the rMD structures was measured by the $R_1^x$ factor, calculated using CORMA. The refined structures were analyzed using DIALS AND WINDOWS 1.0 (*66*).

## RESULTS

*Thermodynamic Stability of the R- and S(61,3)C Mismatches as a Function of pH*. Both the R- and S(61,3)C adducted mismatches exhibited stability which was dependent upon pH. In both instances, $T_m$ values increased at lower pH. However, even at low pH, the observed $T_m$ values were less than for the unmodified *ras61* oligodeoxynucleotide, consistent with the observation that α-styrene oxide adduct formation at adenine $N^6$ reduced the overall stability of the duplex. At neutral pH, the $T_m$ for the R(61,3)C adduct was 27 °C, whereas, for the S(61,3)C adduct, the $T_m$ was 25 °C. Thus, at neutral pH, both the modified mismatches at position (61,3)C had comparable stability. The pH-dependent stability of the R- and S(61,3)C adducts was predicted by studies of A·C mismatch pairs, for which increased $T_m$ at lower pH was attributed to wobble pairing between N1-protonated adenine and cytosine (*37*). This contrasted with the R- and S(61,2)C mismatches, for which the mismatched α-$N^6$ adenyl styrene oxide-modified nucleotide was located one position upstream in the codon 61 sequence. Neither the R- nor S(61,2)C mismatched duplexes exhibited a pH dependence, suggesting that protonated wobble pairing did not occur for those mismatched adducts (*51*). NMR spectra for the R- and S(61,3)C mismatched duplexes were reasonably well-resolved at neutral pH (Figure 1). It was thus of interest to compare the solution structures of the R- and S(61,3)C mismatches with the corresponding R- and S(61,2)C mismatches which had been reported at neutral pH (*51*).

*Assignments of the Nonexchangeable Protons*. Nonexchangeable proton resonance assignments were made using standard methods (*67*, *68*), from data collected at 750 MHz and at temperatures between 15 and 25 °C. Figure 1 shows the sequential NOESY connectivities for the two mismatched adducted duplexes. The assignments are tabulated in Tables S1 and S3 of the Supporting Information.

*(a) R(61,3)C Adduct*. Both $A^6$ H8 and H1′ were broadened, suggesting that the presence of $^{R-SO}A^7$ disrupted base pair $A^6$·$T^{17}$. This was most noticeable at nucleotide $A^6$, since in the complementary strand of this duplex, the sequential NOE cross-peaks were well-resolved. However, cross-peak $C^{15}$ H1′ → $C^{16}$ H6 was weak in the 250 ms mixing time spectrum. In the 80 ms mixing time spectrum, cross-peaks $C^5$ H1′ → $A^6$ H8, $A^6$ H8 → $A^6$ H1′, $A^6$ H1′→$^{R-SO}A^7$ H8, and $C^{16}$ H1′ → $T^{17}$ H6 were not observed.

*(b) S(61,3)C Adduct.* A complete set of sequential connectivities was observed for the adducted strand, although accompanied by several large chemical shift changes at the adduct site. The cross-peaks $C^5$ H6 → $A^6$ H8 and $A^6$ H1′ → $^{S-SO}A^7$ H8 were weak, both at 250 ms and 80 ms. The $^{S-SO}A^7$ H1′ and $G^8$ H1′ resonances underwent upfield shifts, to 5.34 and 5.10 ppm, respectively. For the complementary strand, a complete set of sequential connectivities was observed. However, the cross-peaks $C^{15}$ H6 → $C^{15}$ H1′, $C^{15}$ H1′ → $C^{16}$ H6, and $C^{16}$ H1′ → $T^{17}$ H6 were weak. This suggested motional averaging affecting the $C^{15}$ H1′ proton and a greater-than-normal distance between $C^{16}$ H1′ and $T^{17}$ H6.

*Assignments of the Exchangeable Protons*. *(a) R(61,3)C Adduct.* An expansion of the NOESY data is shown in Figure 2A. At the mismatch site, no imino proton was present. The $T^{17}$ N3H resonance was observed as a broad signal at 13.4

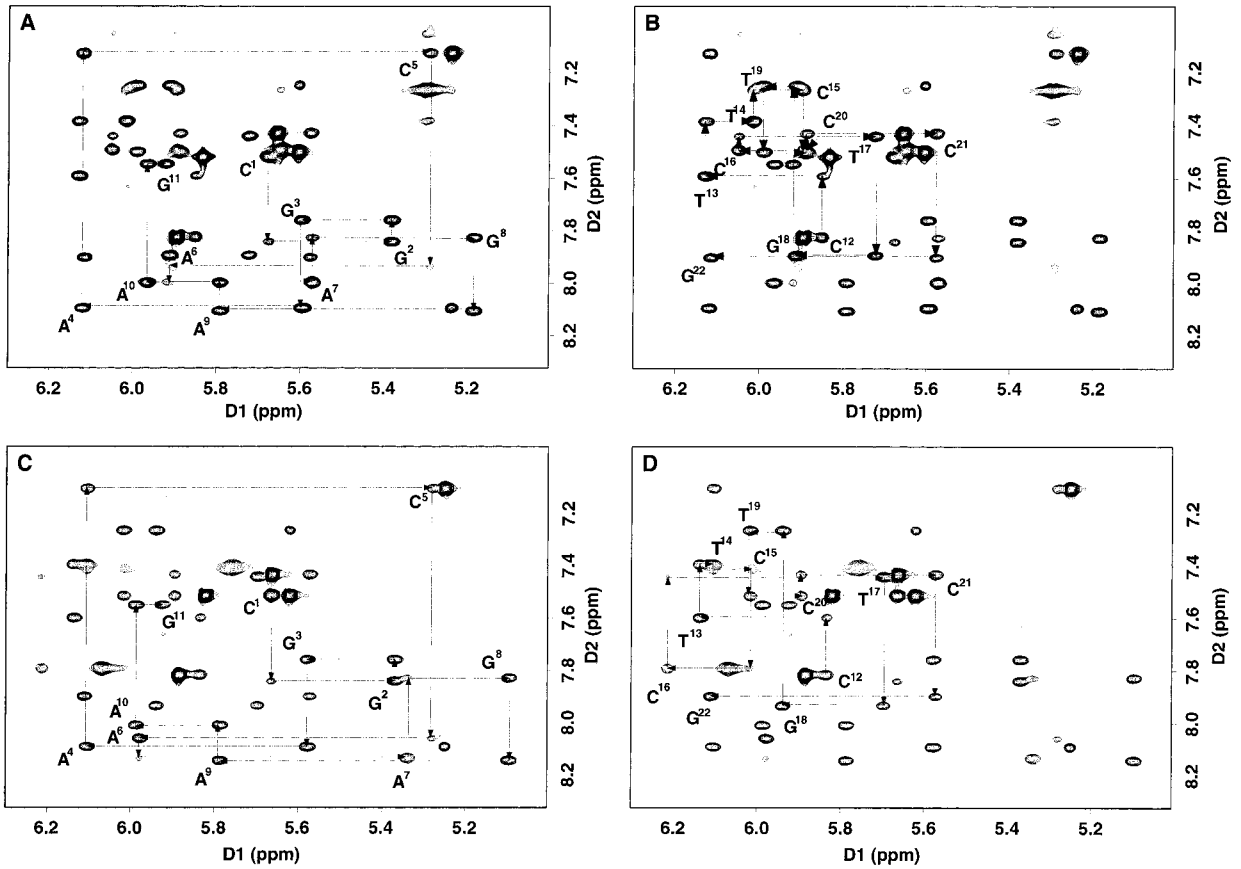


FIGURE 1: Expanded plots of phase sensitive NOESY spectra in $D_2O$ buffer (pH 7.0) at a mixing time of 250 ms showing sequential NOE connectivities from the aromatic to anomeric protons. (A) Nucleotides $C^1 \rightarrow G^{11}$ of the R(61,3)C adduct. (B) Nucleotides $C^{12} \rightarrow G^{22}$ of the R(61,3)C adduct. (C) Nucleotides $C^1 \rightarrow G^{11}$ of the S(61,3)C adduct. (D) Nucleotides $C^{12} \rightarrow G^{22}$ of the S(61,3)C adduct. The base positions are indicated at the intranucleotide cross-peak of the aromatic proton to its own anomeric proton.

ppm (not observed at the contour level shown in Figure 2; a 1D spectrum at 10 °C is included as Figure S1 in the Supporting Information), suggesting increased exchange with solvent. A very weak $T^{17}$ N3H → $G^{18}$ N1H NOESY cross-peak was observed. The N1H resonances of the terminal residues $G^{11}$ and $G^{22}$ were weak signals at 10 °C. They disappeared at temperatures above 15 °C. The observation of anticipated connectivities $G^2$ N1H → $G^3$ N1H → $T^{19}$ N3H → $G^{18}$ N1H and $G^8$ N1H → $T^{14}$ N3H → $T^{13}$ N3H suggested that distortion of the DNA duplex was localized at base pairs $A^6$•$T^{17}$ and $^{R-SO}A^7$•$C^{16}$. The chemical shifts of $G^8$ N1H and $G^{18}$ N1H changed to 12.7 and 12.6 ppm, respectively; $G^8$ N1H was broadened. $G^8$ N1H showed a NOESY cross-peak with $A^9$ H2 but not with $^{R-SO}A^7$ H2. The cross-peak $G^8$ N1H → $T^{14}$ $CH_3$ was not observed. However, $G^8$ N1H → $T^{14}$ N3H was observed as a weak cross-peak. A weak cross-peak was observed between $T^{17}$ N3H → $A^6$ H2. The intranucleotide NOESY cross-peaks between hydrogen-bonded amino protons to H5 protons in the same cytosines were observed. The intraamino cross-peaks for $C^{15}$ and $C^{16}$ were not observed. The assignments are tabulated in Table S4 of the Supporting Information.

*(b) S(61,3)C Adduct*. An expansion of the NOESY data is shown in Figure 2B. At the mismatch site, no imino proton was present. As for the R(61,3)C adduct, the N1H resonances of the terminal residues $G^{11}$ and $G^{22}$ were weak at 10 °C. They disappeared at temperatures above 15 °C. The anticipated NOESY connectivities were observed between $G^2$ → $G^3$ → $T^{19}$ → $G^{18}$ and $G^8$ → $T^{14}$ → $T^{13}$, with a break occurring at $G^{18} \rightarrow T^{17}$ and at the $^{S-SO}A^7$•$C^{16}$ mismatch. No signal was observed for $T^{17}$ N3H, either in 1D or 2D spectra. The chemical shifts of $G^8$ N1H and $G^{18}$ N1H changed to 12.4 and 12.7 ppm, respectively. The cross-peak $G^8$ N1H → $^{S-SO}A^7$ H2 was of greater intensity than the cross-peaks $G^{18}$ N1H → $A^4$ H2 and $G^{18}$ N1H → $A^6$ H2. The assignments are tabulated in Table S2 of the Supporting Information.

*Assignments of the Styrene Protons*. *(a) R(61,3)C Adduct*. The benzylic proton $H_a$ was identified from the 250 ms NOESY spectra by virtue of a strong cross-peak to the methylene protons $H_{b'}$ and $H_{b''}$ of the $CH_2OH$ group. The $^1H$ NMR chemical shifts of the R−SO protons were $H_a$ ($\delta$ 4.85), $H_{b'}$($\delta$ 3.35), $H_{b''}$ ($\delta$ 3.48), $H_{o,o'}$ ($\delta$ 6.94), $H_{m,m'}$ ($\delta$ 7.05), and $H_p$ ($\delta$ 7.02). A COSY cross-peak was observed between $H_a$ and $H_{b',b''}$. The cross-peak $\delta$ 3.35-$\delta$ 4.85 was more intense than the cross-peak $\delta$ 3.48-$\delta$ 4.85, and the measured vicinal coupling constants were 8.4 and 9.8 Hz, respectively. The averaged geminal coupling constant was ∼16 Hz. The inability to resolve separate resonances for the styrenyl $H_{o,o'}$ and $H_{m,m'}$ protons suggested that the styrene ring was in rapid rotation on the NMR time scale. The OH proton of the styrenyl moiety was not identified.

*(b) S(61,3)C Adduct*. The assignment of the styrene protons $H_a$, $H_{b'}$ and $H_{b''}$, as well as of the phenyl ring protons $H_{o,o'}$, $H_{m,m'}$, and $H_p$, was based on NOEs to nonexchangeable and exchangeable protons and on their COSY and TOCSY interactions. Thus, the benzylic proton $H_a$ was identified from the 250 ms NOESY spectra by virtue of a strong cross-peak to the methylene protons $H_{b'}$ and $H_{b''}$ of the $CH_2OH$ group.

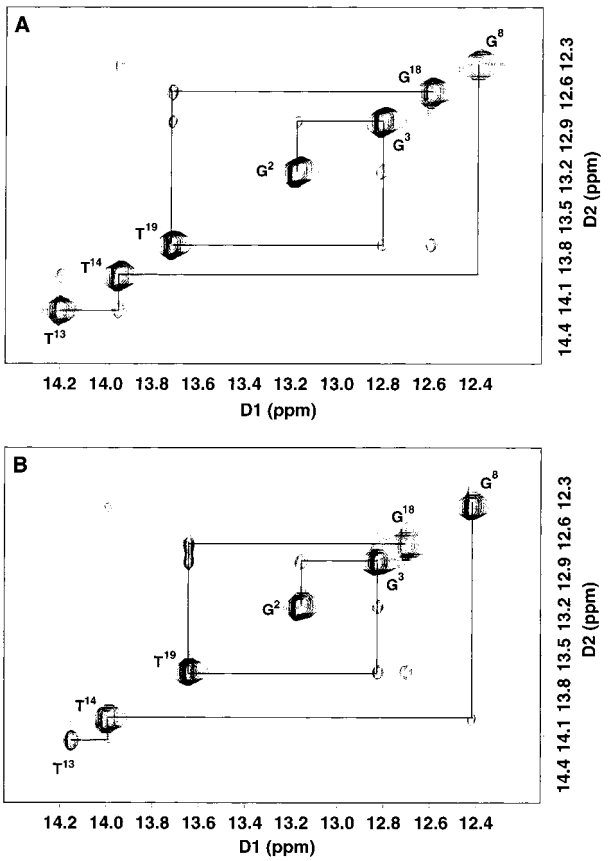


FIGURE 2: Expanded plots of phase sensitive NOESY spectra (pH 7.0) at a mixing time of 200 ms showing NOE connectivities for the imino protons of base pairs $G^2$·$C^{21}$ → $A^{10}$·$T^{13}$ for (A) the R(61,3)C adduct, and (B) the S(61,3)C adduct.

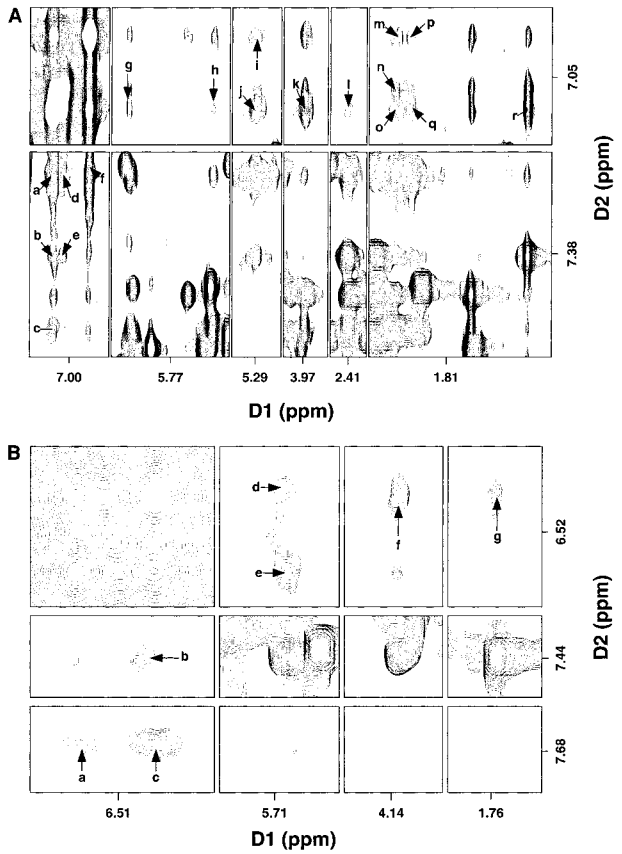


FIGURE 3: NOEs between styrene and DNA protons. (A) The R(61,3)C Adduct. Peaks a, $H_{m,m'}$ → $C^{15}$ H6; b, $H_{m,m'}$ → $T^{14}$ H6; c, $H_{m,m'}$ → $C^{16}$ H6; d, $H_p$ → $C^{15}$ H6; e, $H_p$ → $T^{14}$ H6; f, $H_{o,o'}$ → $C^{15}$ H6; g, $H_{m,m'}$ → $C^{15}$ H1′; h, $H_{m,m'}$ → $C^{16}$ H5; i, $H_{o,o'}$ → $C^{15}$ H5; j, $H_{m,m'}$ → $C^{15}$ H5; k, $H_{m,m'}$ → $C^{15}$ H5″; l, $H_{m,m'}$ → $T^{14}$ H2″; m, $H_{o,o'}$ → $C^{15}$ H2″; n, $H_p$ → $C^{15}$ H2″; o, $H_{m,m'}$ → $C^{15}$ H2″; p, $H_{o,o'}$ → $C^{15}$ H2′; q, $H_{m,m'}$ → $C^{15}$ H2′; r, $H_{m,m'}$ → $T^{14}$ $CH_3$. (B) The S(61,3)C Adduct. Peaks a, $H_p$ → $A^6$ H2; b, $H_{m'}$ → $T^{17}$ H6; c, $H_m$ → $A^6$ H2; d, $H_m$ → $T^{17}$ H1′; e, $H_p$ → $T^{17}$ H1′; f, $H_{m'}$ → $T^{17}$ H4′; g, $H_m$ → $T^{17}$ $CH_3$.

The $^1$H NMR chemical shifts of the S−SO protons were $H_a$ (δ 4.29), $H_{b'}$(δ 3.62), $H_{b''}$ (δ 3.65), $H_{o,o'}$ (δ 6.27), $H_m$ (δ 6.48), $H_{m'}$ (δ 6.50), and $H_p$ (δ 6.57). The hydroxyl proton was observed at 6.72 ppm. NOESY cross-peaks were observed from the OH proton to $H_o$, $H_{m'}$, CH, and $CH_2$ protons. The resolved resonances for the $H_m$ and $H_{m'}$ protons of the styrene ring suggested that the styrene ring was in an ordered environment, with the styrene ring in slow rotation on the NMR time scale. The observation of the hydroxyl proton suggested the existence of an energetically favored orientation for the hydroxyl group.

*NOEs Between the Styrene and the DNA. (a) R(61,3)C Adduct.* Cross-peaks between the styrenyl protons and the DNA protons were observed to the modified base pair $^{R-SO}A^7$·$C^{16}$ and in the 3′ direction, to base pairs $G^8$·$C^{15}$ and $A^9$·$T^{14}$. The greatest number of styrene-DNA cross-peaks were observed for $H_{m,m'}$ of styrene, which exhibited cross-peaks to both $C^{15}$ and $C^{16}$ H5 and H6. In addition, $H_{m,m'}$ showed cross-peaks to a number of deoxyribose protons, including $C^{15}$ H1′, H2′, H2″, and H5′,5″. $H_p$ showed cross-peaks to $T^{14}$ $CH_3$ and $C^{15}$ H6 and H2″. $H_{o,o'}$ also showed a cross-peak to $T^{14}$ $CH_3$, and a number of cross-peaks to $C^{15}$, including $C^{15}$ H5 and H6 and $C^{15}$ H2′,H2″. No cross-peaks were found between the styrenyl moiety and exchangeable protons of the DNA. Figure 3A shows a number of the cross-peaks that were observed.

*(b) S(61,3)C Adduct.* Cross-peaks between the styrenyl protons and the DNA protons were observed to the modified base pair $^{R-SO}A^7$·$C^{16}$ and in the 5′ direction, to base pair $A^6$·$T^{17}$. Of the styrene aromatic protons, $H_p$ showed cross-peaks to $A^6$ H2 and $T^{17}$ H1′, while $H_m$ showed cross-peaks to $A^6$ H2, $T^{17}$ H1′, and $T^{17}$ $CH_3$ and $H_{m'}$ showed cross-peaks to $T^{17}$ H4′ and H6. The latter series of cross-peaks for $H_p$, $H_m$, and $H_{m'}$ was surprising due to the location of adenine H2 and H4′ in the minor groove and thymine $CH_3$ in the major groove of B-DNA. In the $^1$H spectrum obtained in $H_2O$, a series of cross-peaks was observed from $G^8$ N1H to $H_o$, CH, and $CH_2$ of the styrenyl moiety. The methylene protons $H_{b,b'}$ also exhibited NOEs to the DNA, suggesting that the $CH_2OH$ group was fixed in space as opposed to freely rotating. $H_{b'}$ showed NOEs to $C^{15}$ H2″ and $T^{17}$ $CH_3$, while $H_{b''}$ showed an NOE to $T^{17}$ $CH_3$. Figure 3B shows a number of the cross-peaks that were observed.

*DNA Chemical Shift Perturbations. (a) R(61,3)C Adduct.* The chemical shifts induced by this adduct as compared to the unmodified (61,3)C oligodeoxynucleotide at pH 7.9, are shown in Figure 4. The substantial structural perturbation of the R(61,3)C adduct was evidenced by chemical shift changes that spanned a total of four base pairs, from $C^5$·$G^{18}$ → $A^9$·$T^{14}$. These were particularly noticeable in the deoxyribose chemical shifts. Of the DNA base aromatic protons, upfield shifts were observed for $A^6$ H2 and $C^{15}$ H5 and H6. These were in each instance on the order of 0.2 ppm. For the deoxyribose protons, both $C^{15}$ and $C^{16}$ H1′ showed

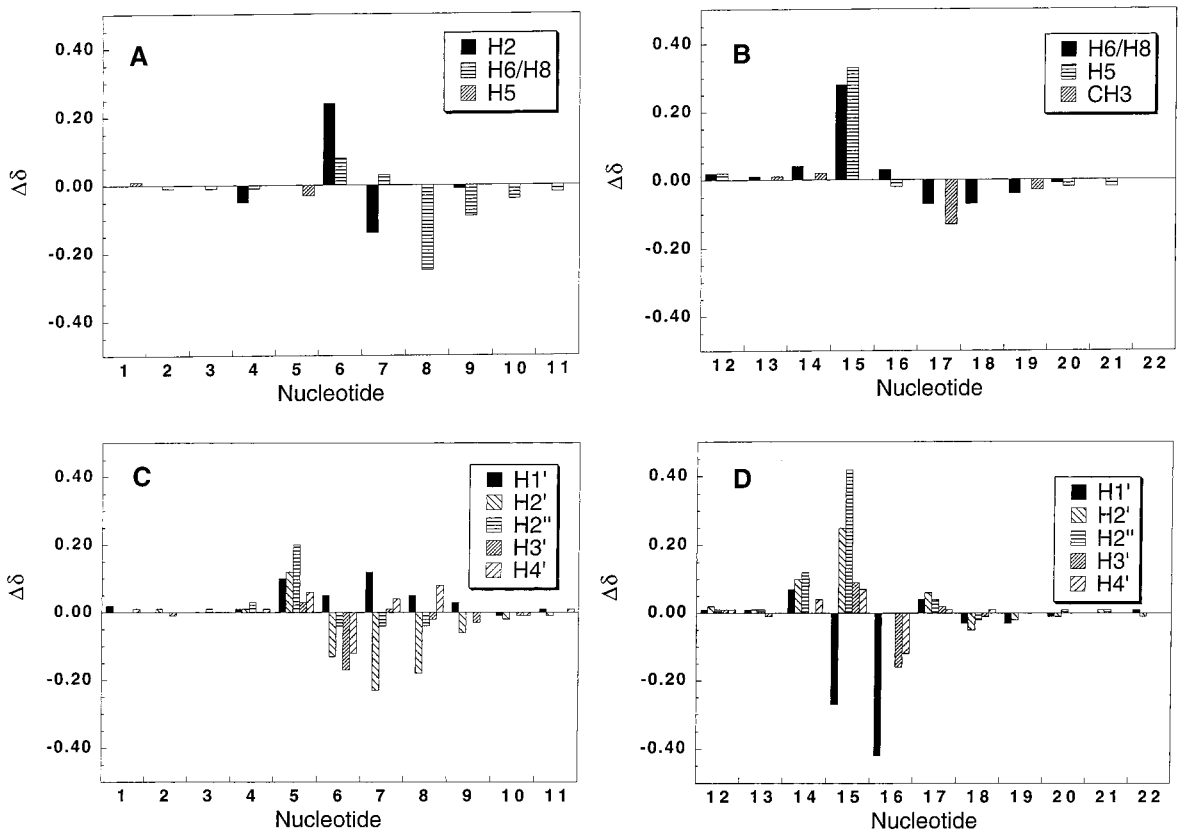


FIGURE 4: Chemical shift differences of selected protons of the R(61,3)C adduct relative to the unmodified mismatched oligodeoxynucleotide (61,3)C. (A) Base aromatic protons in the modified strand. (B) Base aromatic protons in the complementary strand. (C) Deoxyribose protons in the modified strand. (D) Deoxyribose protons in the complementary strand. Upfield shifts are positive.

downfield shifts, on the order of 0.2 and 0.4 ppm, respectively. At $C^{15}$, the remainder of the deoxyribose protons showed upfield chemical shifts of various magnitudes; the largest of these was $C^{15}$ H2″ at 0.40 ppm. The chemical shift perturbations of the deoxyribose protons at $T^{14}$ and $C^{15}$, and upfield chemical shifts for the $C^{15}$ H5 and H6 resonances, were consistent with the notion that the styrenyl moiety was oriented in the 3′-direction from $^{R-SO}A^7$.

*(b) S(61,3)C Adduct*. The chemical shifts induced by this adduct as compared to the unmodified (61,3)C mismatch oligodeoxynucleotide at pH 7.9 are shown in Figure 5. These changes spanned four base pairs $C^5 \cdot G^{18} \rightarrow A^9 \cdot T^{14}$, again suggesting the S(61,3)C adduct induced a substantial structural perturbation to the DNA duplex. The most prominent effect was the substantial deshielding of both $C^{15}$ and $C^{16}$ H5 and H6. At $C^{15}$, $C^{15}$H5 was deshielded by 0.15 ppm and $C^{15}$ H6 was deshielded by 0.45 ppm. At $C^{16}$, $C^{16}$ H5 was deshielded by 0.3 ppm and $C^{16}$ H6 was deshielded by 0.40 ppm.

*Restrained Molecular Dynamics. (a) R(61,3)C Adduct*. The experimental distance set consisted of 313 distances calculated by MARDIGRAS. Additionally, 190 torsion angle restraints, 41 hydrogen-bonding restraints, and 22 base-pairing restraints were included. Excluding the terminal base pairs, an average of 26 restraints were obtained for each base pair. The styrene-DNA cross-peaks included both first and second-order contributions from $H_o$, $H_m$, and $H_p$ and $H_{o'}$ and $H_{m'}$. A total of 566 restraints were used for rMD calculations (Figure 6).

Sets of randomly seeded calculations were carried out starting from either IniA or two separate IniB structures. The two IniB structures differed in the location of the SO moiety. In one instance, the SO moiety was placed in the 5′ direction, while in the other instance, the SO was placed in the 3′ direction. The structural difference between IniA and the two IniB starting structures was confirmed by rmsd values of 4−10 Å. The rMD calculations were run without hydrogen-bonding restraints imposed on $A^6 \cdot T^{17}$ and the $^{R-SO}A^7 \cdot C^{16}$ mispair. The resulting rMD structures were averaged and energy minimized to obtain the final rMD structure (Figure 7). The calculations in all instances converged to structures more similar to the IniB starting structures, as indicated by rmsd comparison of the emergent structures to IniA and IniB. The emergent structures from a set of calculations started from IniA and two IniB structures differed from IniA by rmsd values of 6.7, 8.2, and 8.2 Å, respectively. On the other hand, these same calculations differed from IniB by rmsd values of 2.7, 2.2, and 2.2 Å, respectively. The final structures from each set were tested for convergence by all-atom pairwise rmsd comparison with and without end base pairs. The average rmsd was 0.64 Å, and the maximum rmsd between the two most differing structures was 0.77 Å. To determine whether the structures emergent from the rMD calculations were determined by the experimental distance restraints, control calculations were run. These included only planarity and hydrogen-bonding empirical restraints, only backbone dihedral angles ($\alpha$, $\beta$, $\gamma$, $\epsilon$, and $\zeta$ as loose restraints), or only distance restraints, without the sugar and backbone restraints. The structures obtained without incorporation of experimental distance restraints failed to converge and were at significantly higher energy. The structural refinement procedure defined a family of closely related

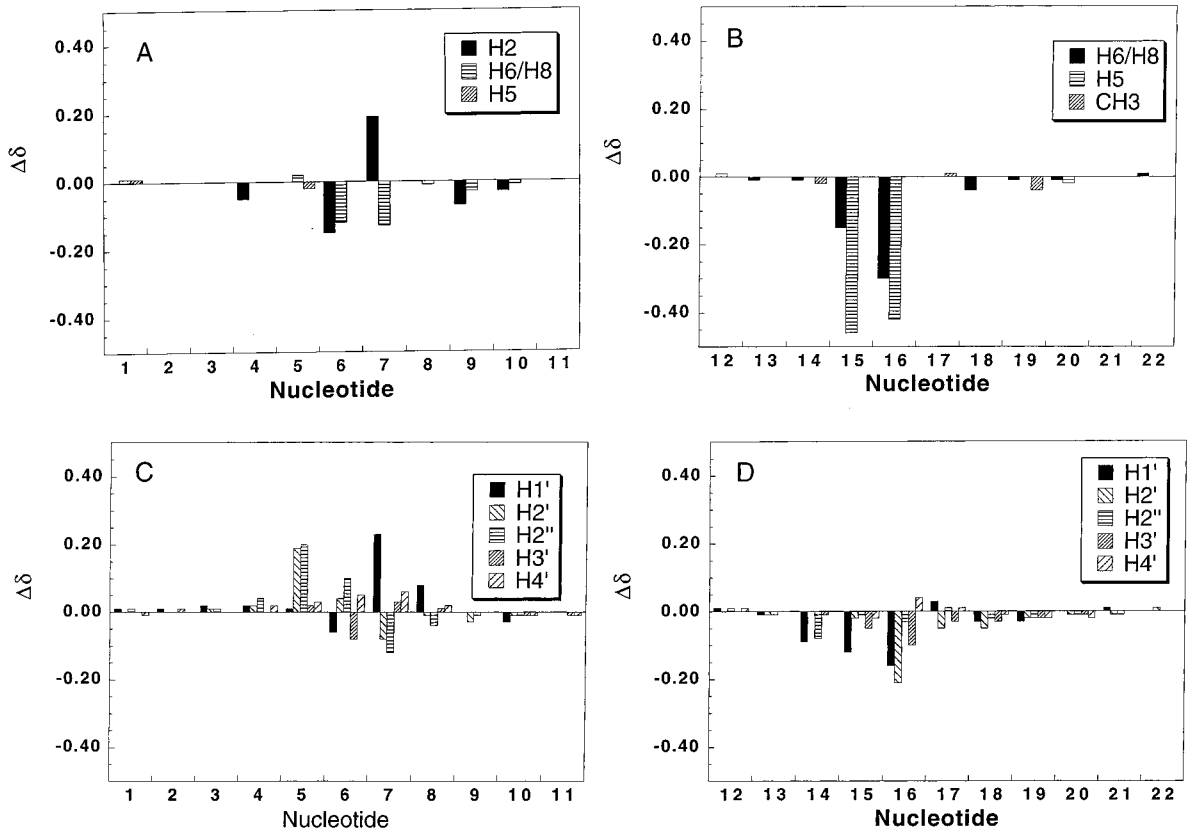


FIGURE 5: Chemical shift differences of selected protons of the S(61,3)C adduct relative to the unmodified mismatched oligodeoxynucleotide (61,3)C. (A) Base aromatic protons in the modified strand. (B) Base aromatic protons in the complementary strand. (C) Deoxyribose protons in the modified strand. (D) Deoxyribose protons in the complementary strand. Upfield shifts are positive.

structures with reasonably good precision, independent of the starting coordinates.

*(b) S(61,3)C Adduct*. The final experimental distance set consisted of 530 distances calculated by MARDIGRAS. Additionally, 190 torsion angle restraints, 41 hydrogen-bonding restraints, and 22 base pair restraints were included. Excluding the terminal base pairs, an average of 35 restraints were obtained for each base pair. The styrene-DNA cross-peaks included both first- and second-order contributions from $H_o$, $H_m$, and $H_p$ and $H_{o'}$ and $H_{m'}$. There were 783 restraints used for rMD calculations. Of these, 22 were base pair restraints and 15 were styrene-DNA restraints (Figure 6). Base step restraints were not used.

Sets of randomly seeded calculations were carried out starting from either IniA or IniB structures. The rMD calculations were run without hydrogen-bonding restraints imposed on $A^6$·$T^{17}$ and the $^{R-SO}A^7$·$C^{16}$ mispair. The resulting rMD structures were averaged and energy minimized to obtain the final rMD structure (Figure 8). The emergent structures did not show great similarity to either IniA or IniB starting structures, suggesting that the S(61,3)C adduct deviated significantly from canonical A- or B-form DNA at the lesion site. The structures emergent from the IniA calculations showed rmsd to IniA of 4.73 Å, and they showed rmsd to IniB of 4.97 Å. Likewise, the structures emergent from the IniB calculations showed rmsd to IniA of 5.6 Å, whereas they showed rmsd to IniB of 3.7 Å. There was satisfactory convergence from either starting structure. The average rmsd was 0.75 Å. In this intance, as well, control experiments revealed that the structures obtained without incorporation of experimental distance restraints were at significantly higher energy and thus judged to be unreasonable. Thus, the structural refinement procedure defined a family of closely related structures with reasonably good precision, independent of the starting coordinates. The resulting rMD structures were averaged and energy minimized to obtain the final rMD structure (Figure 7).

*Complete Relaxation Matrix Calculations*. The accuracy of structures emergent from the rMD calculations was evaluated by comparing the sixth root residuals between theoretical NOE intensities calculated for the emergent structures and the NMR data (Table 1 and Figure S2 in the Supporting Information). Consistent measurements of $R_1^x$ were obtained at each of the three mixing times, with the best values being observed for the longer mixing time data obtained at 750 MHz.

*(a) R(61,3)C Adduct*. The $R_1^x$ factor for the final rMD structure was $10 \times 10^{-2}$. This represented a significant improvement as compared to the IniA or the two IniB starting structures. The $R_1^x$ factor for IniA was $18.7 \times 10^{-2}$, whereas the $R_1^x$ factors for the two IniB starting structures were $15.4 \times 10^{-2}$ and $15.6 \times 10^{-2}$, respectively. Most of the improvement in $R_1^x$ factor came from the internucleotide distances at and adjacent to the adduct site. The internucleotide $R_1^x$ factors for the three starting structures were all $>20 \times 10^{-2}$. The results were consistent with the notion that the cytosine mismatch R(61,3)C adduct deviated significantly from canonical DNA structure at the lesion site. Moreover, they suggested that the refined family of structures were in reasonable agreement with the NOE-based experimental restraints.

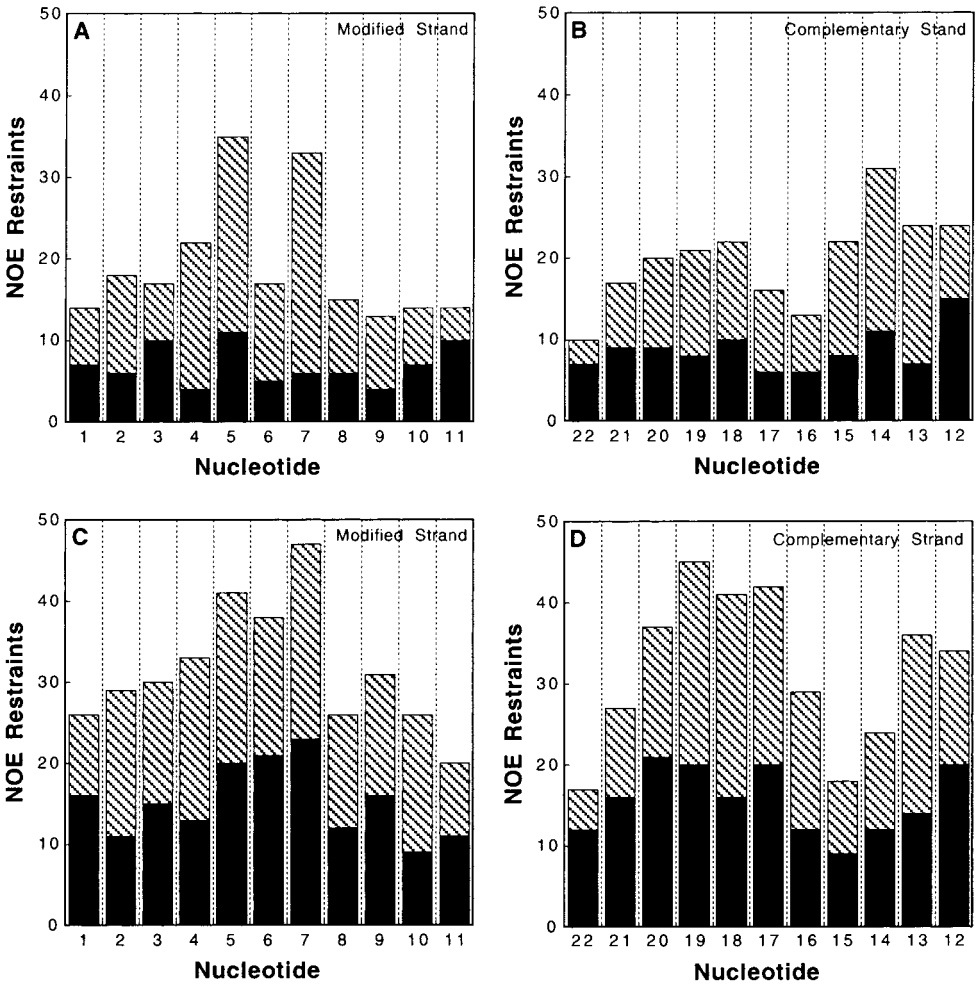


FIGURE 6: Distribution of NOE restraints between nucleotide units of (A) the modified strand of the R(61,3)C adduct, (B) the complementary strand of the R(61,3)C adduct, (C) the modified strand of the S(61,3) adduct, and (D) the modified strand of the S(61,3) adduct. The solid bars represent intranucleotide restraints. The striped bars represent internucleotide restraints.

*(b) S(61,3)C Adduct.* The $R_1^x$ factor for the final rMD structure was $12.2 \times 10^{-2}$. Most of the improvement in the $R_1^x$ factor achieved by the rMD calculations, as compared to the IniA and IniB starting structures, was realized in the internucleotide NOEs. Thus, the IniA and IniB starting structures showed $R_1^x$ factors of $19 \times 10^{-2}$ and $16 \times 10^{-2}$, respectively, while in the emergent structures, these were improved to $11 \times 10^{-2}$. Thus, the calculations substantially improved the fit of the internucleotide distances at the adduct site, to the experimental NOE data. The results suggested that the refined family of structures was in reasonable agreement with the NOE-based experimental restraints.

## DISCUSSION

The consequences of mispairing the R- and S-α-styrene oxide lesions opposite cytosine at positions $A^6$ and $A^7$ of the *ras61* oligodeoxynucleotide differed. Unlike the R- and S(61,2)C adducts (*51*), the structures of the R- and S(61,3)C adducts exhibited a pH dependence and showed lower thermodynamic stability and greater structural perturbation at neutral pH. These changes can be observed in Figure 8. For both the R- and S(61,3)C mismatched oligodeoxynucleotides, rotation about the C6−$N^6$ bond occurred at the modified $A^7$ nucleotide. Consequently, the relative orientations of the styrenyl moieties in relationship to the DNA helix were inverted. The R−SO adduct now faced in the 3′ direction while the S−SO adduct faced in the 5′-direction from the adduct site. Moreover, these structural differences correlated with differential processing of these lesions at the (61,2) vs (61,3) positions of the *ras61* oligodeoxynucleotide, as revealed by site-specific mutagenesis experiments in vivo (*32*).

*Structures of the R- and S(61,3)C Mismatched Adducts. (a) R(61,3)C Adduct.* Rotation of this adduct about the C6−$N^6$ bond as compared to the R(61,3) adduct (*48*, *50*) oriented the styrenyl moiety in the 3′-direction relative to $^{R-SO}A^7$. The rMD calculations predicted that the mismatched base $C^{16}$ was stacked below rather than in the plane of $^{R-SO}A^7$, causing the modified duplex to be unwound with respect to B-DNA. In addition, base pair $A^6$•$T^{17}$ was disrupted. The lowest energy orientation of the styrene moiety was in the major groove, with the aromatic ring flat in the groove and approximately orthogonal to the edges of the DNA bases. This was consistent with the inability to separately resolve the styrene aromatic resonances $H_{o,o'}$ and $H_{m,m'}$ in the $^1H$ spectrum, which suggested rapid flipping of the aromatic ring on the NMR time scale. The predicted orientation of the styrenyl moiety in the 3′-direction relative to $^{R-SO}A^7$ was also supported by NOE data. The refined structure explained the NOE from the styrenyl moiety to $T^{14}$ $CH_3$, which was in the second base pair 3′ to the lesion. The failure to observe NOEs between the styrenyl moiety and DNA exchangeable

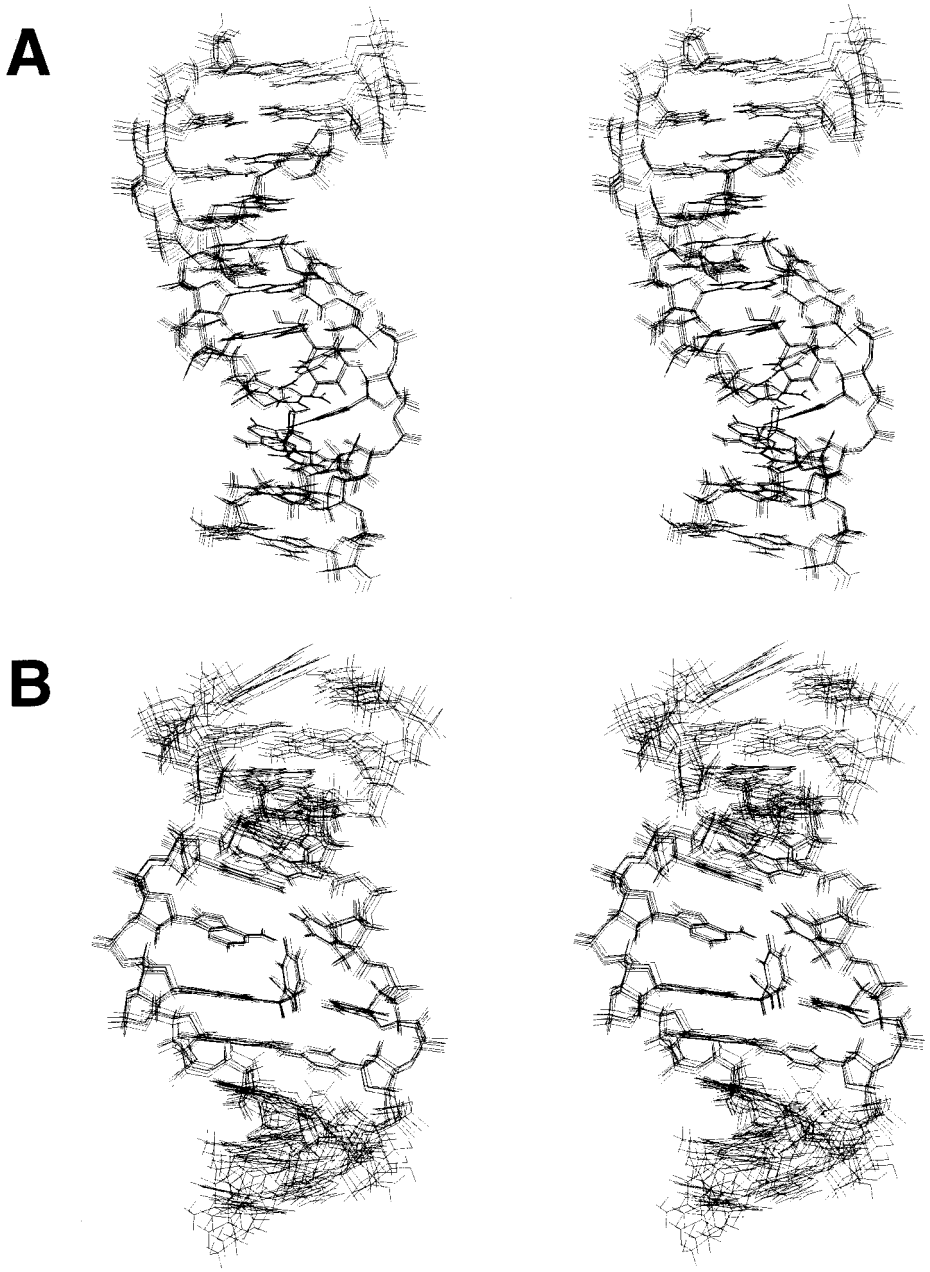


FIGURE 7: Stereoviews of (A) six structures emergent from randomly seeded rMD calculations for the R(61,3)C adduct, and (B) six structures emergent from randomly seeded rMD calculations for the S(61,3)C adduct.

protons further served to position the styrene ring in the major groove. The upfield chemical shifts of $C^{15}$ H5 and H6, compared to the remainder of the cytosine H5 and H6 resonances, were consistent with the 3′-orientation of the styrene ring. These were attributed to the styrene ring shielding effect. In the structures emergent from rMD calculations, $C^{15}$ H5 and H6 were located beneath the styrene ring. The observation of NOEs between $C^{16}$ H5 and H6 and $H_{m,m'}$ of SO confirmed the proximity between SO and $C^{16}$. The lack of significant chemical shift perturbations for $C^{16}$ H5 and H6 was therefore somewhat surprising. This suggested that $C^{16}$ was likely to be shifted further toward the major groove than predicted by the rMD calculations. That would have the effect of pulling $C^{16}$ H5 and H6 further away from the shielding cone of the styrenyl ring while still maintaining NOE contact between these protons and the styrenyl ring protons. The calculations predicted backbone angle distortions at and immediately adjacent to $^{R-SO}A^7$, which were consistent with the spectroscopic indications of structural perturbations at the lesion site and the 5′-neighbor base pair. The ~0.5 ppm downfield shifts of styrene aromatic resonances $H_{o,o'}$, $H_{m,m'}$, and $H_p$ were attributed to deshielding by mispaired $C^{16}$, which was approximately orthogonal to the styrenyl moiety. The $H_a$ resonance shifted downfield to 4.85 ppm, attributed to the ring current effect of $^{R-SO}A^7$. The lack of Watson−Crick hydrogen bonding at $^{R-SO}A^7$·$C^{16}$, and disruption of hydrogen bonding at 5′-neighbor $A^6$·$T^{17}$, was consistent with the very weak $T^{17}$ N3H → $G^{18}$ N1H NOE cross-peak observed in the NMR data. Although the OH proton of the styrenyl moiety was not identified, the rMD calculations predicted the favored conformation about the $N^6-C_\alpha-C_\beta-O$ torsion angle was stabilized by a gauche-type interaction between the hydroxyl and adenine $N^6$ at the lesion site.

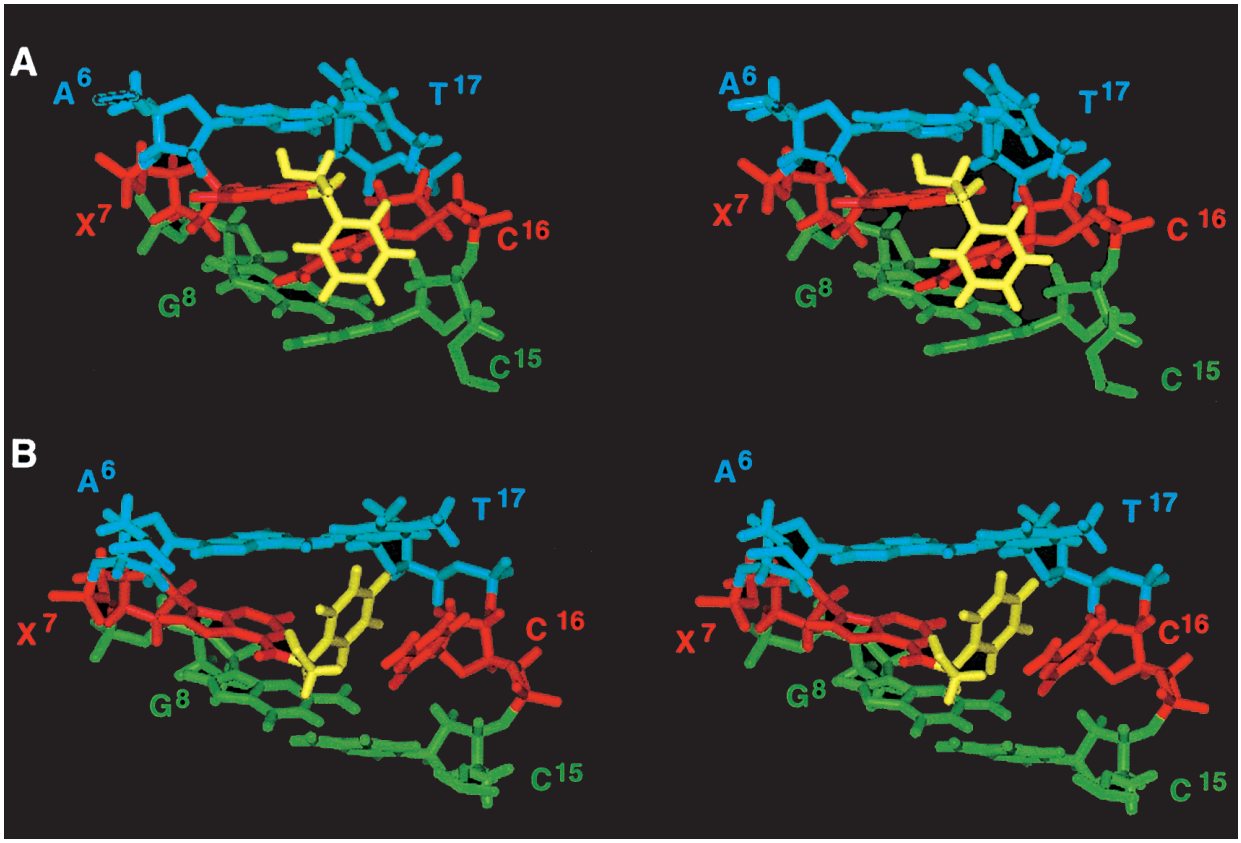


FIGURE 8: Orientation of the styrenyl moiety at the lesion site in the *ras61* oligodeoxynucleotide at neutral pH, as predicted by rMD calculations. Stereoviews. (A) The R(61,3)C adduct. The styrenyl moiety (yellow) is oriented such that the aromatic ring remains in the major groove and is facing the 3′-direction from the lesion site. Base pair $A^6$•$T^{17}$ (blue) is disrupted. The mismatched base $C^{16}$ (red) stacks below the modified base $X^7$ (red). Base pair $G^8$•$C^{15}$ (green) is intact but suffers increased buckle away from the lesion site. (B) The S(61,3)C adduct. The styrenyl moiety (yellow) is inserted into the DNA duplex, such that the aromatic ring is facing the 5′-direction from the lesion site. Base pair $A^6$•$T^{17}$ (blue) is disrupted. The mismatched base $C^{16}$ (red) is pushed toward the major groove. Base pair $G^8$•$C^{15}$ (green) is intact.

*(b) S(61,3)C Adduct.* The major structural perturbations occurred at the lesion site $^{S-SO}A^7$•$C^{16}$ and its 5′-neighbor $A^6$•$T^{17}$. Rotation of this adduct about the C6−$N^6$ bond as compared to the S(61,3) adduct (*49*, *50*) had two effects. First, it reoriented the styrenyl moiety in the 5′-direction relative to $^{S-SO}A^7$. Second, it located the 5′-oriented styrene ring in a binding pocket within the DNA duplex. This pocket was not intercalative, i.e., the styrenyl moiety remained approximately perpendicular to the DNA helical axis, disrupting the 5′-neighbor base pair $A^6$•$T^{17}$. $T^{17}$ was shifted toward the major groove. The formation of a binding pocket in the DNA was consistent with the $^1$H data that suggested the styrene ring was in an ordered environment with ring flips occurring slowly on the NMR time scale. This orientation of the styrene moiety explained the failure to observe the $T^{17}$ N3H resonance in the $^1$H spectrum. Loss of Watson−Crick hydrogen bonding between $A^6$ N1 and $T^{17}$ N3H was attributed to the shift of $T^{17}$ toward the major groove. The formation of a binding pocket in the interior of the DNA duplex was consistent with the unusual pattern of NOEs between the styrene moiety and the DNA, which involved both major and minor groove DNA protons. An example of this was the observation of NOE interactions between the styrene aromatic protons to minor groove DNA protons $A^6$ H2 and $T^{17}$ H1′. Simultaneously, NOEs between the styrene aromatic protons and $T^{17}$ $CH_3$, located in the major groove, suggested that the binding pocket must have access to both grooves of the DNA. This was corroborated by unusual NOEs from the imino proton $G^8$ N1H to $H_o$, CH, and $CH_2$. These NOEs also would not have been consistent with a major groove location for the styrenyl moiety. The calculations predicted backbone angle distortions at and adjacent to $^{S-SO}A^7$. Good stacking interactions were predicted between $A^6$, $^{S-SO}A^7$, and $G^8$. The deshielding of the $C^{16}$ H5 and H6 resonances was consistent with the peculiar displacement of $T^{17}$ into the major groove to accommodate insertion of the styrenyl moiety into the DNA helix. The ∼0.5 ppm upfield shifts of the adduct aromatic proton resonances $H_{o,o'}$, $H_{m,m'}$, and $H_p$ were attributed to shielding by $T^{17}$. The ability to observe the OH proton of the styrenyl moiety suggested it was in slow exchange. The rMD calculations predicted that the favored conformation of the $N^6$−$C_\alpha$−$C_\beta$ −O torsion angle was stabilized by a gauche-type interaction between the hydroxyl and adenine $N^6$ at the lesion site.

*Rotation at the C6−$N^6$ Bond.* Perhaps the most striking observation regarding the structures of the R- and S(61,3)C mismatched oligodeoxynucleotides was the conformation at the C5−C6−$N^6$−$C_\alpha$ torsion angle as predicted by the rMD calculations. In both instances, it was calculated to be 5 ± 5°. This placed the NH proton at adenine $N^6$ facing into the major groove. Consequently, it was not positioned to hydrogen bond with $C^{16}$, the mismatched nucleotide complementary to the modified adenine. This differed from previously examined adenine $N^6$ styrene oxide adducts (*10*−*14*), for which the C5−C6−$N^6$−$C_\alpha$ torsion angle was consistently ∼180°. The latter conformation placed styrene oxide adducts

Table 1: Analysis of the rMD-Generated Structures of the R(61,3)C and S(61,3)C Adducts

| NMR restraints | R(61,3)C adduct | S(61,3)C adduct |
|---|---|---|
| total no. of distance restraints | 313 | 530 |
| interresidue distance restraints | 140 | 191 |
| intraresidue distance restraints | 173 | 339 |
| DNA−SO distance restraints | 20 | 15 |
| empirical restraints | | |
| H-bonding restraints | 41 | 41 |
| dihedral planarity restraints | 22 | 22 |
| sugar pucker restraints | 110 | 110 |
| backbone torsion angle restraints | 80 | 80 |
| structural statistics | | |
| NMR *R*-factor ($R_1^x$)[a,b,c] | | |
| IniA | 0.187 | 0.159 |
| IniB | 0.154 | 0.149 |
| ⟨rMDAi⟩ | 0.0993 | 0.131 |
| ⟨rMDBi⟩ | 0.0100 | 0.122 |
| rmsd of NOE violations (Å) | 0.037 | 0.037 |
| no. of NOE violations > 0.2 Å (entire duplex) | 0 | 0 |
| root-mean-square deviations from ideal geometry | | |
| bond length (Å) | 0.008 | 0.007 |
| bond angle (deg) | 1.80 | 1.82 |
| improper angle (deg) | 0.71 | 0.51 |
| pairwise rmsd (Å) over all atoms | | |
| IniA vs IniB | 7.98 | 7.15 |
| IniB vs ⟨rMDBi⟩ | 2.21 | 3.67 |
| IniA vs ⟨rMDAi⟩ | 6.72 | 4.73 |
| ⟨rMDBi⟩ vs ⟨rMDAi⟩ | 1.70 | 1.66 |

[a] The mixing time was 250 ms. [b] $R_1^x = \sum |(a_o)_i^{1/6} - (a_c)_i^{1/6}| / \sum |(a_o)_i^{1/6}|$, where ($a_o$) and ($a_c$) are the intensities of observed (nonzero) and calculated NOE cross-peaks. [c] IniA, starting energy-minimized A-DNA with the SO moiety; IniB, starting energy-minimized B-DNA with the SO moiety, ⟨rMDAi⟩ , average of 6 rMD structures starting from IniA; ⟨rMDBi⟩ , average of 6 MD structures starting from IniB.

at adenine $N^6$ in the major groove and solvent exposed (*48*−*51*). The solvent-exposed location for the styrene ring in the major groove might be predicted to energetically unfavorable. Indeed, the adenine $N^6$ styrene adducts differed from the sterically larger and more hydrophobic adenine $N^6$ PAH adducts, which consistently intercalated (*69*−*76*). The present results suggest that rotation about the C6−$N^6$ bond, especially in the case of the S(61,3)C adduct, allows the styrene ring to be accommodated in a more hydrophobic pocket within the DNA duplex. We surmise that this does not occur for the correctly paired R- and S(61,3) adducts because favorable maintenance of Watson−Crick base pairing compensates for the energetic penalty associated with placing the styrenyl moiety in the major groove.

These mismatched R- and S(61,3)C structures were examined at neutral pH. Consequently, protonation of either $^{R-SO}A^6$ or $^{S-SO}A^6$ N1 at the lesion site, to form the protonated A·C mismatch, was disfavored. This was consistent with the structural results in which rotation about the C6−$N^6$ bond placed the styrene moiety into the helix and thus prevented the NH proton from participating in hydrogen bonding with mismatched $C^{16}$ in the complementary strand. However, UV melting curves for both the R- and S(61,3)C adducts showed a pH dependence, consistent with potential formation of protonated A·C mismatches at lower pH. It seems unlikely if such protonated mismatches formed at lower pH that the styrenyl moiety would remain inserted into the DNA helix. It will thus be of interest to determine if rotation about the C6−$N^6$ bond is pH dependent.

*Flanking Base Effect.* The observation that rotation about the C6−$N^6$ bond was not observed in the R- and S(61,2)C adducts revealed a "flanking base effect" in the structure of these mismatched cytosine opposite these styrene oxide adducts in the *ras61* oligodeoxynucleotide. This suggested that the identity of the 5′-neighbor base pair, which must be disrupted in order for rotation about the C6−$N^6$ bond to occur, was crucial. The 5′-neighbor A·T base pair was apparently more easily disrupted than the 5′-neighbor C·G base pair to the R- and S(61,2)C lesions. A similar "flanking base effect" was reported for benzo[*a*]pyrene adducts at guanine $N^2$. In that instance, it was proposed that a less stable A·T flanking base pair as compared to a G·C flanking base pair might provide greater "local flexibility" (*77*, *78*).

*Biological Implications.* The structural data reveal a correlation between the biological processing of the R- and S(61,2) and R- and S(61,3) styrene oxide adducts and the structures of these adducts in duplex DNA when mispaired with cytosine. Site-specific mutagenesis studies in which the *ras61* sequence was modified at the R- and S(61,2) and R- and S(61,3) positions revealed low levels of A → G transitions only for the S(61,2) adduct (*32*). The R- and S(61,3) adducts were nonmutagenic and readily bypassed by a number of polymerases (*32*). The A → G transitions result from incorrect incorporation of cytosine opposite the modified adenine; thus, the structures of cytosine mismatched with these SO adducts were of interest. The present results reveal that cytosine mismatches opposite the R- and S(61,3) SO adducts exhibited entirely different structures as compared to the corresponding cytosine mismatches opposite the R- and S(61,2) adducts. Significantly, among the previously examined R- and S(61,2)C adducts (*51*), and the presently examined R- and S(61,3)C adducts, only the S(61,2)C adduct mispaired with cytosine to form an ordered structure in which the $N^6$-modified adenine shifted toward the minor groove (*51*). The S(61,2)C adduct did not form a protonated A·C pair. This suggested hydrogen bonding between the incoming dNTP and the DNA template was not prerequisite to the genesis of α-SO-induced A → G mutations at that site. It inferred that base-pairing geometry was of greater importance. With regard to the R- and S(61,3) adducts that were observed to be nonmutagenic, we hypothesize that to the extent that cytosine might be incorrectly inserted at this site, subsequent rotation of the styrenyl moiety about the C6−$N^6$ bond and resulting structural distortion is not conducive toward successful polymerase extension beyond the damage site, accounting for the failure to observe A → G mutations at this site.

*Summary*. The orientation of the adenyl $N^6$ SO-adduct depends on whether it is placed complementary in the DNA duplex to the correct nucleotide thymine or the incorrect nucleotide cytosine and the identity of the 5′-neighbor base pair. These factors appear to govern an exquisite balance of thermodynamics involving base stacking, hydrogen bonding, and rotation about the C6−$N^6$ bond of the $N^6$-modified adenosine. The rotation about the C6−$N^6$ bond which occurred when the R- and S(61,3) α-SO adducts were mispaired with cytosine provides a potential explanation as to why low levels of A → G mutations, observed for the S(61,2) α-SO adduct, were not observed for the R- and S(61,3) adducts.

## ACKNOWLEDGMENT

Mr. Markus Voehler assisted with NMR spectroscopy. Dr. Sherry L. Painter and Professor R. Stephen Lloyd (The University of Texas Medical Branch, Galveston) provided helpful discussions. Mr. Zhijun Li and Ms. Mary Kerske assisted with the preparation of the manuscript.

## SUPPORTING INFORMATION AVAILABLE

Tables S1, the chemical shifts of the nonexchangeable protons of the S(61,3)C adduct, S2, the chemical shifts of the nonexchangeable protons of the S(61,3)C adduct, S3, the chemical shifts of the exchangeable protons of the R(61,3)C adduct, and S4, the chemical shifts of the exchangeable protons of the S(613)C adduct. It also contains Figures S1, 1D spectra of the imino region of the two adducts at 10 °C, and S2, inverse sixth root residuals calculated for the average structures emergent from rMD calculations. This material is available free of charge via the Internet at http://pubs.acs.org.

## REFERENCES

1. de Meester, C., Poncelet, F., Roberfroid, M., Rondelet, J., and Mercier, M. (1977) *Mutat. Res. 56*, 147−152.
2. Wade, D. R., Airy, S. C., and Sinsheimer, J. E. (1978) *Mutat. Res. 58*, 217−223.
3. Bonatti, S., Abbondandolo, A., Corti, G., Fiorio, R., and Mazzaccaro, A. (1978) *Mutat. Res. 52*, 295−300.
4. Ott, M. G., Kolesar, R. C., Schamweber, H. C., Schneider, E. J., and Venable, J. R. (1980) *J. Occup. Med. 22*, 445−460.
5. Hodgson, J. T., and Jones, P. D. (1985) *J. Work Environ. 11*, 347−352.
6. Matanoski, G. M., and Schwarts, L. (1987) *J. Occup. Med. 29*, 675−680.
7. Wong, O. (1990) *J. Ind. Med. 47*, 753−762.
8. Harris, C., Philpot, R. M., Hernandez, O., and Bend, J. R. (1986) *J. Pharmacol. Exp. Theor. 236*, 144−149.
9. Foureman, G. L., Harris, C., Guengerich, F. P., and Bend, J. R. (1989) *J. Pharmacol. Exp. Theor. 248*, 492−497.
10. Elovaara, E., Engstrom, K., Nakajima, T., Park, S. S., Gelboin, H. V., and Vainio, H. (1991) *Xenobiotica 21*, 651−661.
11. Guengerich, F. P., Kim, D.-H., and Iwasaki, M. (1991) *Chem. Res. Toxicol. 4*, 168−179.
12. Guengerich, F. P. (1992) *FASEB J. 6*, 745−748.
13. Nelson, D. R., Kamataki, T., Waxman, D. J., Guengerich, F. P., Estabrook, R. W., Feyereisen, R., Gonzalez, F. J., Coon, M. J., Gunsalus, I. C., Goto, O., Okuda, K., and Nebert, D. W. (1993) *DNA Cell Biol. 10*, 1−51.
14. Nakajima, T., Elovaara, E., Gonzalez, F. J., Gelboin, H. V., Raunio, H., Pelkonen, O., Vainio, H., and Aoyama, T. (1994) *Chem. Res. Toxicol. 7*, 891−896.
15. Nakajima, T., Wang, R.-S., Elovaara, E., Gonzalez, F. J., Gelboin, H. V., Vainio, H., and Aoyama, T. (1994) *Biochem. Pharmacol. 48*, 637−642.
16. Savela, K., and Hemminki, K. (1986) *Arch. Toxicol. 9* (Suppl.), 281−285.
17. Barlow, T., Takeshita, J., and Dipple, A. (1998) *Chem. Res. Toxicol. 11*, 838−845.
18. Qian, C., and Dipple, A. (1995) *Chem. Res. Toxicol. 8*, 389−395.
19. Latif, F., Moschel, R. C., Hemminki, K., and Dipple, A. (1988) *Chem. Res. Toxicol. 1*, 364−369.
20. Norppa, H., Sorsa, M., Pfaffli, P., and Vainio, H. (1980) *Carcinogenesis 1*, 357−361.
21. Norppa, H., Hemminki, K., Sorsa, M., and Vainio, H. (1981) *Mutat. Res. 91*, 243−250.
22. Horvath, E., Prongracz, K., Rappaport, S., and Bodell, W. J. (1994) *Carcinogenesis 15*, 1309−1315.
23. Vodicka, P., Vodickova, L., and Hemminki, K. (1993) *Carcinogenesis 14*, 2059−2061.
24. Vodicka, P., Vodickova, L., Trejbalova, K., Scram, R. J., and Hemminki, K. (1994) *Carcinogenesis 15*, 1949−1953.
25. Vodicka, P., Bastlova, T., Vodickova, L., Peterkova, K., Lambert, B., and Hemminki, K. (1995) *Carcinogenesis 16*, 1473−1481.
26. Bastlova, T., Vodicka, P., Peterkova, K., Hemminki, K., and Lambert, B. (1995) *Carcinogenesis 16*, 2357−2362.
27. Bastlova, T., and Podlutsky, A. (1996) *Mutagenesis 11*, 581−591.
28. Longnecker, D. S., and Terhune, P. G.(1998) *Pancreas 17. 17*, 323−4.
29. Fearon, E. R., and Vogelstein, B. (1990) *Cell 61*, 759−767.
30. Loeb, L. A., and Christians, F. C. (1996) *Mutat. Res. 19* (350), 279−286.
31. Jen, J., Powell, S. M., Papadopoulos, N., Smith, K. J., Hamilton, S. R., Vogelstein, B., and Kinzler, K. W.(1994) *Cancer Res. 54*, 5523−5526.
32. Latham, G. J., Zhou, L., Harris, C. M., Harris, T. M., and Lloyd, R. S. (1993) *J. Biol. Chem. 268*, 23427−23434.
33. Chary, P., Latham, G. J., Robberson, D. L., Kim, S. J., Han, S., Harris, C. M., Harris, T. M., and Lloyd, R. S. (1995) *J. Biol. Chem. 270*, 4990−5000.
34. McNees, A. G., O'Donnell, M., Horton, P. H., Kim, H. Y., Kim, S. J., Harris, C. M., Harris, T. M., and Lloyd, R. S. (1997) *J. Biol. Chem. 272*, 33211−33219.
35. Patel, D. J., Kozlowski, S. A., Ikuta, S., and Itakura, K. (1984) *Biochemistry 23*, 3218−3226.
36. Patel, D. J., Kozlowski, S. A., Ikuta, S., and Itakura, K. (1984) *Fed. Proc. 43*, 2663−2670.
37. Hunter, W. N., Brown, T., Anand, N. N., and Kennard, O. (1986) *Nature 320*, 552−555.
38. Kennard, O. (1986) *Biochem. Soc. Trans. 14*, 207−210.
39. Gao, X., and Patel, D. J. (1987) *J. Biol. Chem. 262*, 16973−16984.
40. Hunter, W. N., Brown, T., and Kennard, O. (1987) *Nucleic Acids Res. 15*, 6589−6606.
41. Kalnik, M. W., Kouchakdjian, M., Li, B. F. L., Swann, P. F., and Patel, D. J. (1988) *Biochemistry 27*, 100−108.
42. Brown, T., Leonard, G. A., Booth, E. D., and Kneale, G. (1990) *J. Mol. Biol. 212*, 437−440.
43. Wang, C., Gao, H., Gaffney, B. L., and Jones, R. A. (1991) *J. Am. Chem. Soc. 113*, 5486−5488.
44. Boulard, Y., Cognet, J. A. H., Gabarro-Arpa, J., Le Bret, M., Sowers, L. C., and Fazakerley, G. V. (1992) *Nucleic Acids Res. 20*, 1933−1941.
45. Fazakerley, G. V., and Boulard, Y. (1995) *Methods Enzymol. 261*, 145−163.
46. Boulard, Y., Cognet, J. A., Gabarro-Arpa, J., Le Bret, M., Carbonnaux, C., and Fazakerley, G. V. (1995) *J. Mol. Biol. 246*, 194−208.
47. Feng, B., and Stone, M. P. (1995) *Chem. Res. Toxicol. 8*, 821−832.
48. Feng, B., Zhou, L., Passarelli, M., Harris, C. M., Harris, T. M., and Stone, M. P. (1995) *Biochemistry 34*, 14021−14036.
49. Feng, B., Voehler, M. W., Zhou, L., Passarelli, M., Harris, C. M., Harris, T. M., and Stone, M. P. (1996) *Biochemistry 35*, 7316−7329.
50. Stone, M. P., and Feng, B. (1996) *Magn. Reson. Chem. 34*, S105−S114.
51. Painter, S. L., Zegar, I. S., Tamura, P. J., Bluhm, S., Harris, C. M., Harris, T. M., and Stone, M. P. (1999) *Biochemistry 38*, 8635−8646.
52. Harris, C. M., Zhou, L., Strand, E. A., and Harris, T. M. (1991) *J. Am. Chem. Soc. 113*, 4328−4329.
53. Borer, P. N. (1975) *Handbook of biochemistry and molecular biology*, CRC Press, Cleveland.
54. Piotto, M., Saudek, V., and Sklenar, V. (1992) *J. Mol. Biol. 6*, 661−665.
55. Brunger, A. T. (1992) *X-Plor. Version 3.1. A system for X-ray Crystallography and NMR*, Yale University Press, New Haven.
56. Borgias, B. A., and James, T. L. (1990) *J. Magn. Reson. 87*, 475−487.
57. Liu, H., Tonelli, M., and James, T. L. (1996) *J. Magn. Reson. B 111*, 85−89.

58. Schmitz, U., and James, T. L. (1995) *Methods Enzymol. 261*, 3−44.
59. Rinkel, L. J., and Altona, C. (1987) *J. Biomol. Struct. Dyn. 4*, 621−649.
60. Pikkemaat, J. A., and Altona, C. (1996) *Magn. Reson. Chem. 34*, S33−S39.
61. Kim, S. G., Lin, L. J., and Reid, B. R. (1992) *Biochemistry 31*, 3564−3574.
62. Saenger, W. (1984) *Principles of Nucleic Acid Structure*, Springer-Verlag, New York.
63. Tisne, C., Simenel, C., Hantz, E., Schaeffer, F., and Delepierre, M. (1996) *Magn. Reson. Chem. 34*, S115−S124.
64. Brooks, B. R., Bruccoleri, R. E., Olafson, B. D., States, D. J., Swaminathan, S., and Karplus, M. (1983) *J. Comput. Chem. 4*, 187−217.
65. Keepers, J. W., and James, T. L. (1984) *J. Magn. Reson. 57*, 404−426.
66. Ravishankar, G., Swaminathan, S., Beveridge, D. L., Lavery, R., and Sklenar, H. (1989) *J. Biomol. Struct. Dyn. 6*, 669−699.
67. Reid, B. R. (1987) *Q. Rev. Biophys. 20*, 2−28.
68. Patel, D. J., Shapiro, L., and Hare, D. (1987) *Q. Rev. Biophys. 20*, 35−112.
69. Cosman, M., Fiala, R., Hingerty, B. E., Laryea, A., Lee, H., Harvey, R. G., Amin, S., Geacintov, N. E., Broyde, S., and Patel, D. (1993) *Biochemistry 32*, 2488−2497.
70. Cosman, M., Laryea, A., Fiala, R., Hingerty, B. E., Amin, S., Geacintov, N. E., Broyde, S., and Patel, D. J. (1995) *Biochemistry 34*, 1295−1307.
71. Schurter, E. J., Sayer, J. M., Oh-hara, T., Yeh, H. J. C., Yagi, H., Luxon, B. A., Jerina, D. M., and Gorenstein, D. G. (1995) *Biochemistry 34*, 9009−9020.
72. Schurter, E. J., Yeh, H. J. C., Sayer, J. M., Lakshman, M. K., Yagi, H., Jerina, D. M., and Gorenstein, D. G. (1995) *Biochemistry 34*, 1364−1375.
73. Yeh, H. J. C., Sayer, J. M., Liu, X., Altieri, A. S., Byrd, R. A., Lakshman, M. K., Yagi, H., Schurter, E. J., Gorenstein, D. G., and Jerina, D. M. (1995) *Biochemistry 34*, 13570−13581.
74. Zegar, I. S., Kim, S. J., Johansen, T. N., Horton, P., Harris, C. M., Harris, T. M., and Stone, M. P. (1996) *Biochemistry 35*, 6212−6224.
75. Schwartz, J. L., Rice, J. S., Luxon, B. A., Sayer, J. M., Xie, G., Yeh, H. J., Liu, X., Jerina, D. M., and Gorenstein, D. G. (1997) *Biochemistry 36*, 11069−11076.
76. Zegar, I. S., Chary, P., Jabil, R. J., Tamura, P. J., Johansen, T. N., Lloyd, R. S., Harris, C. M., Harris, T. M., and Stone, M. P. (1998) *Biochemistry 37*, 16516−16528.
77. Geacintov, N. E., Cosman, M., Hingerty, B. E., Amin, S., Broyde, S., and Patel, D. J. (1997) *Chem. Res. Toxicol. 10*, 111−146.
78. Suh, M., Jankowiak, R., Ariese, F., Mao, B., Geacintov, N. E., and Small, G. J. (1994) *Carcinogenesis 15*, 2891−2898.

BI992080T